Journal Pre-proof

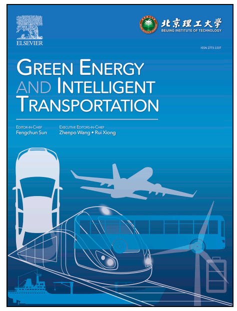

Low-frequency Consensus knowledge Transfer in PEM Fuel Cells for Cross-Domain Online Voltage Degradation Prediction

Hangyu Wu, Fulin Fan, Wenbo Hao, Kai Song, Rui Xue, Jinhai Jiang, Chuanyu Sun, Yang Li, Changjun Xie, Siew Hwa Chan

PII: S2773-1537(26)00017-4

DOI: https://doi.org/10.1016/j.geits.2026.100405

Reference: GEITS 100405

To appear in: *Green Energy and Intelligent Transportation*

Received Date: 3 August 2025

Revised Date: 27 January 2026

Accepted Date: 13 February 2026

Please cite this article as: Wu H, Fan F, Hao W, Song K, Xue R, Jiang J, Sun C, Li Y, Xie C, Chan SH, Low-frequency Consensus knowledge Transfer in PEM Fuel Cells for Cross-Domain Online Voltage Degradation Prediction, *Green Energy and Intelligent Transportation*, https://doi.org/10.1016/j.geits.2026.100405.

Low-frequency Consensus knowledge Transfer in PEM Fuel Cells for Cross-Domain Online Voltage Degradation Prediction

Hangyu Wu[1,2], Fulin Fan[1,2*], Wenbo Hao[3], Kai Song[1,2*], Rui Xue[1,2], Jinhai Jiang[1,2], Chuanyu Sun[1,2], Yang Li[4], Changjun Xie[5], Siew Hwa Chan[6]

1 School of Electrical Engineering and Automation, Harbin Institute of Technology, Harbin, 150001, China.

2 Suzhou Research Institute, Harbin Institute of Technology, Suzhou, 215104, China.

3 State Grid Heilongjiang Electric Power Research Institute, Harbin, 150000, China.

4 Department of Electrical Engineering, Chalmers University of Technology, 41296 Gothenburg, Sweden.

5 Wuhan Industrial Technology Institute of Artificial Intelligence and New Energy Vehicles, Wuhan 430119, China.

6 School of Mechanical and Aerospace Engineering, Nanyang Technological University, 50 Nanyang Avenue, Singapore 639798, Singapore.

* Corresponding authors

E-mail address: fulin.fan@hit.edu.cn (F. Fan); kaisong@hit.edu.cn (K. Song)

CRediT authorship contribution statement

Hangyu Wu: Writing - Original Draft, Conceptualization, Validation, Methodology. **Fulin Fan:** Writing - Review & Editing, Supervision. **Wenbo Hao:** Formal analysis. **Kai Song:** Funding acquisition, Supervision. **Rui Xue:** Data Curation. **Jinhai Jiang:** Software, **Chuanyu Sun:** Formal analysis, **Yang Li:** Writing - Review & Editing, Supervision. **Changjun Xie:** Writing - Review & Editing, Supervision. **Siew Hwa Chan:** Writing - Review & Editing,

Acknowledgement

This work was supported by the Key Research & Development Plan of Heilongjiang Province (Grant No. 2024ZXJ03C06).

Data Availability

The data and materials used to support the findings of this study are available from the corresponding author upon reasonable request.

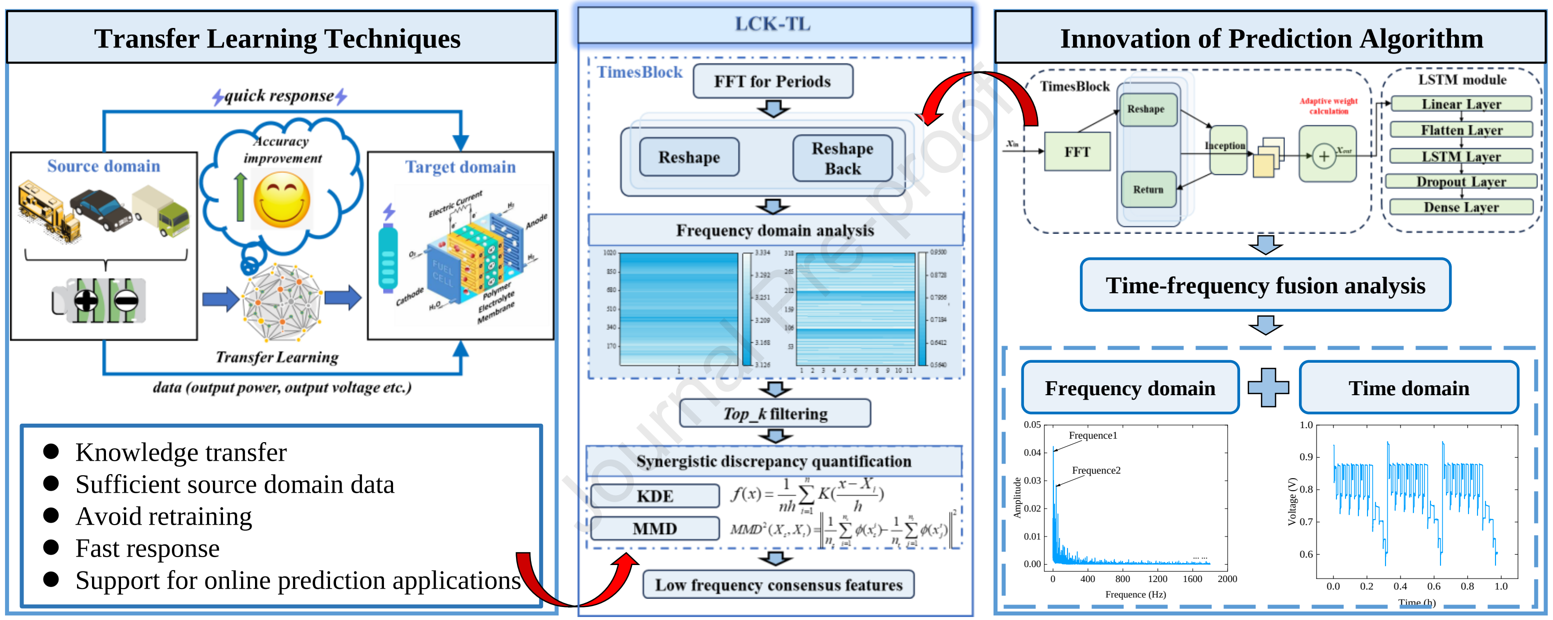

Transfer Learning Techniques
quick response
Accuracy improvement
Source domain
Target domain
Transfer Learning
data (output power, output voltage etc.)
Knowledge transfer
Sufficient source domain data
Avoid retraining
Fast response
Support for online prediction applications
LCK-TL
TimesBlock
FFT for Periods
Reshape
Reshape Back
Frequency domain analysis
Top_k filtering
Synergistic discrepancy quantification
KDE
MMD
Low frequency consensus features
Innovation of Prediction Algorithm
TimesBlock
FFT
Reshape
Inception
Return
Adaptive weight calculation
LSTM module
Linear Layer
Flatten Layer
LSTM Layer
Dropout Layer
Dense Layer
Time-frequency fusion analysis
Frequency domain
Time domain
Frequence1
Frequence2
Amplitude
Frequence (Hz)
Voltage (V)
Time (h)

Low-frequency Consensus Knowledge Transfer in PEM Fuel Cells for Cross-Domain Online Degradation Prediction

Abstract:

Traditional time–frequency domain methods face critical limitations in predicting voltage degradation of proton exchange membrane fuel cells (PEMFCs). Time-domain models struggle to robustly separate long-term degradation-related low-frequency trends from contaminated voltage signals under highly dynamic and non-stationary conditions, while conventional frequency-domain analysis loses essential time-localized information during feature extraction. Both approaches exhibit significantly degraded prediction performance under limited data conditions. To overcome these challenges, this paper proposes a time–frequency fusion algorithm that integrates TimesNet with long short-term memory (LSTM), effectively combining 2D frequency-domain representations with 1D temporal memory to enhance voltage degradation prediction under dynamic conditions. Based on the capability of TimesNet-LSTM to extract low-frequency voltage features, a transfer learning technique grounded in low-frequency consensus knowledge (LCK-TL) is further developed. By selectively transferring low-frequency voltage features that robustly reflect aging patterns, LCK-TL considerably reduces distribution discrepancy between source and target domains, achieving joint optimization of predictive modeling and transfer mechanisms. Leveraging the inherently low computational cost of transfer learning, LCK-TL enables rapid multi-step predictions while maintaining accuracy, providing effective guidance

for cross-device and cross-condition fuel cell health management.

Keywords: Proton exchange membrane fuel cell; Time-frequency fusion; Transfer learning; Dynamic conditions; Online prediction

1. Introduction

1.1 Background and Literature Review

As a core technology in new energy systems, proton exchange membrane fuel cells (PEMFCs) have become a critical solution for hydrogen-powered vehicles, UAV propulsion, and stationary power generation due to their zero-emission characteristics, high energy density, and rapid cold-start capabilities [1,2]. During continuous operation, complex physicochemical changes within PEMFCs lead to nonlinear degradation of stack output performance [3]. Effective prognostics and health management (PHM) strategies are essential to ensure reliable operation and extend service life [4,5]. It is noteworthy that the voltage degradation of PEMFCs serves as a comprehensive external manifestation of the aging processes of its key internal components, directly reflecting the decline in system output performance [6]. Therefore, predicting the voltage degradation trajectory provides an effective means of assessing the overall performance degradation state of the fuel cell [7].

Data-driven methods autonomously model nonlinear relationships between performance degradation and multi-dimensional features by mining large-scale historical operational data, eliminating reliance on complex physicochemical models [8,9]. These methods have emerged as the dominant approaches for degradation predictions. Among them, recurrent neural networks (RNNs) and their variants, with inherent advantages in temporal dependency modeling, have become mainstream solutions to PEMFC degradation forecasting [10,11]. He et al. [12] proposed a novel health indicator extraction method by combining autoencoder and long short-term memory (LSTM) to predict future PEMFC voltages. Wu et al. [13] introduced a bidirectional gated recurrent unit (BiGRU) coupled with a voltage recovery model, enabling online parameter updates via a moving window approach for effective degradation predictions. While composite RNN architectures significantly improve lifespan prediction accuracy, their ability to model time-varying correlations heavily depends on large datasets [14]. In data-scarce scenarios, these models often converge to local optima during training, leading to substantial prediction errors [15,16].

Most data-driven methods primarily focus on gradual degradation analysis of PEMFC output voltage and power in the time domain [17–19]. However, time-domain analysis struggles to characterize millisecond-level voltage transients under dynamic conditions, limiting its effectiveness in capturing short-term anomalies [20]. To address this issue, frequency-domain analysis has been progressively adopted for enhanced dynamic responses. Wang et al. [21] extracted frequency-domain health indicators via Hilbert transform and constructed a symbolic GRU model. Wu et al. [22] proposed an energy-based frequency domain method using empirical mode decomposition and power spectral density to extract health indicators. Wu et al. [23] developed TimesNet for time-series prediction, mapping temporal signals into multi-period coupled frequency representation spaces. This frequency-entangled feature learning mechanism significantly enhances the joint modeling of long-range dependencies and transient behaviors, offering a promising novel paradigm for PEMFC degradation prediction under complex conditions. Sun et al. [24] processed voltage signals using Complete Ensemble Empirical Mode Decomposition and analyzed the potential relationships between voltage signals at different frequencies and fuel cell operating conditions. Their work demonstrated the feasibility of investigating PEMFC aging mechanisms from a voltage frequency-domain perspective. Meng et al. [25] systematically analyzed electrochemical impedance spectra under different cathode stoichiometric ratios. They found that the impedance response in the low-frequency region was significantly correlated with concentration polarization loss. This highlights the high sensitivity of low-frequency signals to mass transport processes. Further research indicates that the intensification of concentration polarization loss is closely related to the decay of the electrochemical active surface area and the increase in equivalent resistance. Together, these two factors reflect the degradation of the membrane electrode assembly, which is the most critical component during PEMFC aging.

To overcome data limitations in deep learning, transfer learning has gained increasing attention [26]. It leverages knowledge from source domains to enhance prediction performance in target domains with limited labeled data [27]. For instance, Zhang et al. [28] combined deep temporal feature extraction with transfer learning, achieving an improved accuracy and reduced computational costs. Yue et al. [29]

introduced a digital twin framework by integrating CNN-LSTM and transfer learning for real-time degradation prediction under static and quasi-static conditions. Tang et al. [30] developed a transfer learning-based online degradation prediction model by using Transformer networks for quasi-static scenarios. Izadi et al. [31] built a WaveNet-GRU architecture with transfer learning to assess PEMFC degradation across same-condition and cross-device scenarios. However, most of the existing transfer learning models focus on transferring knowledge between stacks under similar operating conditions. In real-world dynamic environments, frequent current density fluctuations cause PEMFCs to transition across ohmic, concentration and activation polarization regions [32]. This multi-polarization switching induces dynamically non-stationary voltage signal distributions, which deviates significantly from data patterns under static/quasi-dynamic conditions. Consequently, traditional transfer strategies would fail to adapt to cross-region feature drift, severely limiting generalization performance in complex dynamic settings [33].

1.2 Research gap and contributions

Based on the literature review in Section 1.1, three critical challenges remaining in PEMFC degradation predictions are summarized as below:

1) Existing methods predominantly rely on either time- or frequency-domain feature representations, failing to capture the coupled relationships between transient voltage fluctuations and low-frequency degradation trends under dynamic conditions.

2) Most approaches employ simple cascaded architectures where predictions and

transfer modules are separately optimized, which limits domain adaptation to post-hoc compensation rather than embedding transfer-aware feature learning during model training.

3) Traditional transfer learning assumes homogeneous distributions across static/quasi-dynamic data, though dynamic operation of PEMFC in real world causes time-varying non-stationary feature distributions across multiple polarization regions, significantly undermining model robustness of existing methods.

To systematically address these challenges, this paper proposes a comprehensive PEMFC performance prediction framework that deeply integrates time-frequency modeling with transfer learning. The time-frequency fusion algorithm is first developed to enable accurate degradation forecasting under dynamic conditions. By leveraging its capability of low-frequency feature screening, a cross-domain consensus space is constructed to mitigate inter-domain discrepancies during transfer learning. Then, the low-latency characteristics of transfer learning are utilized to enable online multi-step predictions across devices and operational settings. The main contributions of the work include:

1) The TimesNet-LSTM algorithm is proposed to resolve cross-period modeling challenges for non-stationary temporal signals under dynamic conditions through complementary integration of two-dimensional (2D) frequency-domain representations and one-dimensional (1D) temporal memory.

2) The LCK-TL technique is developed by innovatively leveraging the TimesNet-

LSTM's capability of low-frequency feature analysis to mitigate inter-domain discrepancies, establishing a joint optimization paradigm for prediction algorithms and transfer learning.

3) The proposed TimesNet-LSTM algorithm together with the LCK-TL technique enable knowledge transfer across PEMFC operating conditions and devices, providing end-to-end support for lightweight online prediction applications.

The rest of the paper is structured as follows: Section 2 introduces the proposed PEMFC degradation prediction framework including TimesNet-LSTM and LCK-TL; Section 3 outlines the data sources employed for model training and tests; Section 4 validates the performance of TimesNet-LSTM and LCK-TL in PEMFC degradation predictions; and conclusions are presented in Section 5.

2. Methodology

2.1 PEMFC degradation prediction framework

The proposed PEMFC degradation prediction framework is illustrated in Fig. 1. Experimental data partitioning is first performed by defining the non-dynamic condition dataset from the IEEE PHM 2014 Data Challenge as the source domain, while the dynamic condition data from the Greenlight 20 (G20) test station is designated as the target domain. Then, a novel predictive algorithm is developed by integrating the 2D frequency-domain representation advantages of TimesNet with the 1D temporal memory characteristics of LSTM, with the superiority of the TimesNet-LSTM architecture being validated across multiple dimensions. Building on the cross-condition robustness of low-frequency degradation features extracted by the TimesBlock module within TimesNet-LSTM, the TimesNet-LSTM algorithm is combined with transfer learning (TL) techniques, forming an innovative low-frequency consensus knowledge transfer learning (LCK-TL) method to mitigate the prediction accuracy reductions caused by inter-domain discrepancies. Finally, an online PEMFC degradation prediction model supporting cross-condition and cross-device scenarios is established based on the proposed framework.

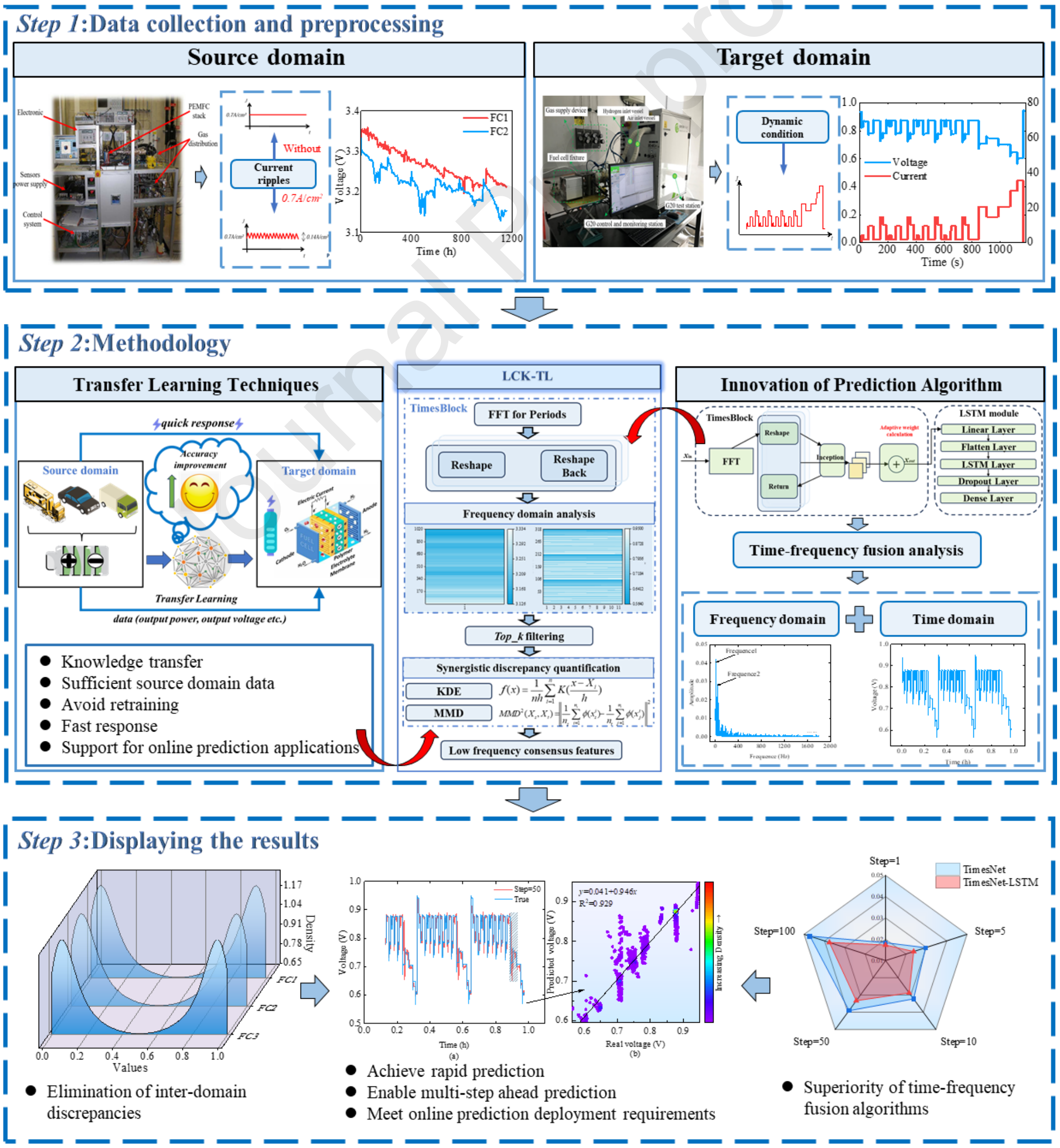

Fig. 1. Schematic of the proposed online PEMFC degradation prediction framework.

2.2 Time-frequency feature fusion algorithm

The proposed time-frequency fusion algorithm, TimesNet-LSTM, integrates the frequency-domain representation of TimesNet with the temporal modeling of LSTM through sequential architecture. Specifically, the TimesBlock employs the Fast Fourier Transform (FFT) to map temporal signals into the frequency domain, where periodic patterns of signals are extracted by multi-scale Inception convolutions. The processed features undergo dimensionality reshaping prior to being adaptively fused with original temporal signals. The flattened hybrid features are then fed into LSTM layers to capture long-term dependencies under dynamic conditions, while subsequent dense layers generate voltage predictions based on complementary time-frequency characteristics. In summary, TimesNet is responsible for extracting features in the local and frequency domains, while LSTM captures long-term trends in the global and temporal domains. Together, they enable the accurate characterization of complex degradation processes under dynamic operating conditions. The architecture of TimesNet-LSTM's fusion mechanism is depicted in Fig. 2.

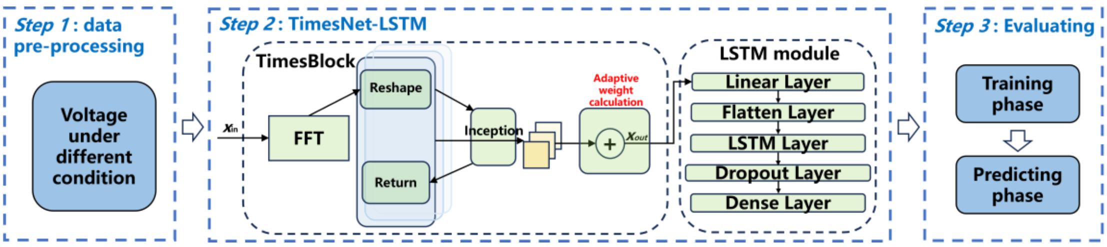

Fig. 2. Architecture of TimesNet-LSTM mechanism for time-frequency fusion.

2.2.1 TimesNet

The TimesNet analyzes PEMFC voltage signals from a novel 2D perspective. The

1D time series is extended into 2D space through its TimesBlock modules, integrating time series analysis with powerful 2D processing architectures from computer vision. The architecture employs Inception module to process 2D tensors, utilizing 2D convolutional kernels of varying sizes to expand receptive fields and enhance model robustness. This approach overcomes the limitations of traditional 1D convolutions by simultaneously capturing intra-period and inter-period temporal variations, thereby significantly improving modeling capabilities. This 2D time-varying modeling capability enables TimesNet to robustly extract features from highly non-stationary and dynamic PEMFC voltage signals. The high-quality features it provides establish a solid foundation for the subsequent LSTM temporal memory module. The network structure of the TimesNet is shown in Fig. 3, where its primary workflow consists of the following four steps:

Step 1：Frequency and periodic information extraction：

The periodicity of time series in temporal dimension is calculated by using the FFT:

$$A = \mathrm{Avg}(\mathrm{Amp}(\mathrm{FFT}(X_{1D}))) \tag{1}$$

$$\{f_1, \dots, f_k\} = \underset{f_* \in \left\{1, \dots, \left[\frac{T}{2}\right]\right\}}{\arg Topk}(A) \tag{2}$$

$$p_i = \left[\frac{T}{f_i}\right], i \in \{1, \dots, k\} \tag{3}$$

where the operator FFT(·) denotes the FFT; Amp(·) computes the amplitude spectrum; and Avg(·) calculates the mean value across c-dimensional features. The term $A \in R^T$ represents the intensity of each frequency component in X_{1D}. The top k amplitudes

(*Topk*) are then selected to obtain the most significant frequencies $\{f_1,\ldots, f_k\}$ with unnormalized amplitudes, which correspond to k periodic lengths $\{p_1,\ldots, p_k\}$.

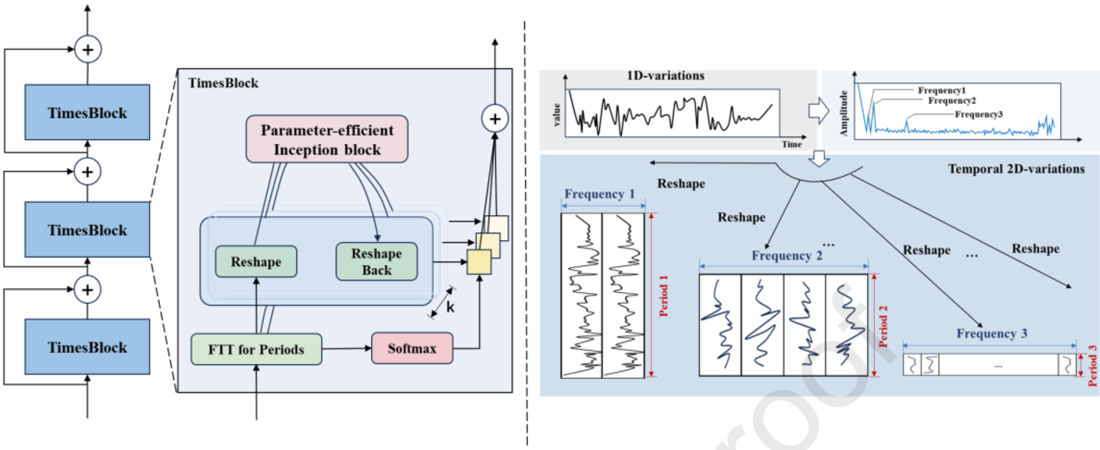

Fig. 3. The network structure of TimesNet.

Step 2： 2D tensor transformation：

The key periodic components and their corresponding frequencies captured by FFT are converted into 2D tensors to represent temporal variations in 2D space. The transformation process is formulated by:

$$X_{2D}^{l,i} = \text{Reshape}_{p_i, f_i}(\text{Padding}(X_{1D}^{l-1})), i \in \{1,\ldots,k\} \tag{4}$$

where Padding$(\cdot)$ denotes zero-padding along the temporal dimension to ensure compatibility with Reshape$_{p_i,f_i}(\cdot)$ where p_i and f_i indicate the row and column dimensions of the transformed 2D tensor, respectively. The term $X_{2D}^{l,i}$ represents the i-th reconstructed temporal sequence based on frequency f.

Step 3： 2D convolutional feature extraction：

The 2D tensor X_{2D}^{i} is then processed by the parameter-efficient Inception$(\cdot)$ to capture multi-scale spatiotemporal patterns, with the use of 2D convolutions for information extraction:

$$\hat{X}_{2D}^{l,i} = \text{Inception}(X_{2D}^{l,i}) \tag{5}$$

Step 4：Conversion of 2D Tensors to 1D Space:

The processed 2D tensor is subsequently transformed back into 1D representations, followed by frequency importance-based weighted fusion:

$$X_{1D}^{l,i} = \text{Trunc}(\text{Reshape}_{1,(p_i,f_i)}(\hat{X}_{2D}^{l,i})) \tag{6}$$

where Trunc(·) denotes the operation that truncates the padded sequence from *Step* 1 to its original length.

2.2.2 LSTM

LSTM is a specialized recurrent neural network (RNN) architecture, primarily designed for processing and forecasting time series data [34]. By incorporating memory cells and gating mechanisms, LSTM selectively retains and discards long-term dependencies, thereby enhancing prediction accuracies for temporal dynamics. The computational formulations governing the gating mechanisms within LSTM are formulated by:

$$f_t = \sigma\left(W_f \cdot \left[h_{t-1}, x_t\right] + b_f\right) \tag{7}$$

$$i_t = \sigma\left(W_i \cdot \left[h_{t-1}, x_t\right] + b_i\right) \tag{8}$$

$$C_t = f_t * C_{t-1} + i_t * \tilde{C}_t \tag{9}$$

$$O_t = \sigma\left(W_o \cdot \left[h_{t-1}, x_t\right] + b_o\right) \tag{10}$$

$$h_t = O_t * \tanh\left(C_t\right) \tag{11}$$

where f_t, i_t, C_t and O_t represent the forget gate, input gate, cell state and output gate, respectively; x_t denotes the input at the current time step; h_t denotes the hidden state;

σ(·) and tanh(·) represent the Sigmoid and hyperbolic tangent activation functions, respectively; W_f, W_i and W_o are weight matrices; and the bias vectors b_f, b_i and b_o correspond to each gating mechanism.

2.3 Time-frequency fusion and knowledge transfer

2.3.1 Transfer learning

Transfer learning aims to enhance target domain prediction by leveraging source domain knowledge, a technique successfully applied to cross-scenario applications like wind power forecasting and photovoltaic output analysis, demonstrating its adaptability to non-stationary time-series data [35]. Given source domain data $D_s = \{(x_1^s, y_1^s), (x_2^s, y_2^s), \dots, (x_i^s, y_i^s)\}_{i=1}^{N_s}$ and target domain data $D_t = \{(x_1^t, y_1^t), (x_2^t, y_2^t), \dots, (x_j^t, y_j^t)\}_{j=1}^{N_t}$, where (x_i^s, y_i^s) and (x_j^t, y_j^t) denote feature-prediction sequence pairs, the core of transfer prediction lies in extracting transferable feature representations and latent patterns from D_s, then adaptively transferring them to D_t with distribution shifts, thereby improving target domain prediction under limited samples.

For PEMFC degradation prediction, transfer learning establishes a cross-scenario lifespan prediction model by constructing a fuel cell system degradation knowledge base from passenger vehicles to commercial vehicles. This approach enables generalized prediction using a single pre-trained model, eliminating per-task retraining while mitigating accuracy degradation caused by insufficient initial operational data.

2.3.2 Low-frequency consensus knowledge

In the context of PEMFC degradation prediction, the voltage signal represents a superposition of the aging trend and fluctuations due to dynamic operating conditions.

High-frequency components are typically dominated by rapid load transients and random noise. Consequently, they are highly sensitive to specific operating conditions. In contrast, low-frequency components characterize the gradual degradation caused by intrinsic physicochemical aging mechanisms. This degradation pattern demonstrates consistency across different devices and operating conditions. Therefore, these low-frequency features form a body of consensus knowledge that is robust to domain shifts, providing a reliable foundation for transfer learning.

During transfer learning, distribution shifts between the source and target domains cause traditional temporal models to fail due to feature mismatches during knowledge transfer. To reduce data distribution discrepancies between the source and target domains, this paper proposes a low-frequency consensus knowledge transfer learning (LCK-TL) technique. LCK-TL achieves cross-domain generalization through the tripartite coupling of the TimesBlock module, kernel density estimation (KDE), maximum mean discrepancy (MMD), and transfer learning. Specifically, the TimesBlock module adjusts the *top_k* parameter to select voltage low-frequency data from the source and target domains. Subsequently, KDE-MMD is applied to quantify the distribution differences between the two domains and identify consensus low-frequency voltage features. Finally, TimesNet-LSTM is trained based on low-frequency consensus knowledge to obtain a pre-trained model for transfer prediction. The cross-domain generalization workflow of LCK-TL is illustrated in Fig. 4.

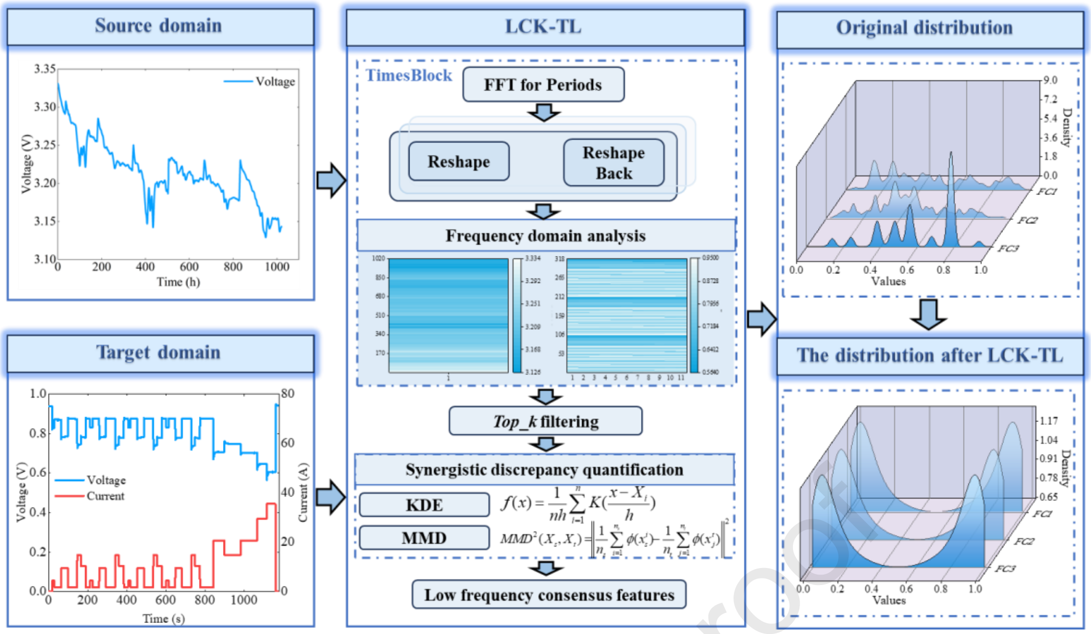

Fig. 4. Workflow of LCK-TL.

KDE is a non-parametric method that applies kernel smoothing to probability density estimation, using a kernel as the weighting function to estimate the probability density function of a random variable. Compared to traditional histogram-based estimation, KDE introduces differentiable kernel functions to model probability density in continuous space, effectively overcoming information loss caused by discrete binning. In domain adaptation analysis, this method visualizes statistical differences by constructing probability density distribution surfaces for the source and target domains. The primary KDE formula is as follows:

$$f(x) = \frac{1}{nh}\sum_{i=1}^{n} K\left(\frac{x - X_i}{h}\right) \tag{12}$$

where $f(x)$ represents the probability density estimate at point x, $K(\cdot)$ is the kernel function, h is the bandwidth parameter, and n is the sample size.

MMD can capture complex nonlinear structures and patterns in time-series data, enabling more accurate data distribution measurement and pattern matching, thus being applicable for calculating distribution differences between source and target domains [36]. Meanwhile, based on the calculation results of MMD, a similarity S is proposed to quantitatively assess the inter-domain differences. The calculation formulas for MMD and similarity S are as follows.:

$$MMD^2(X_s, X_t) = \left\| \frac{1}{n_s} \sum_{i=1}^{n_s} \phi(x_s^i) - \frac{1}{n_t} \sum_{j=1}^{n_t} \phi(x_j^t) \right\|^2 \tag{13}$$

$$S = \frac{1}{1 + MMD^2(X_s, X_t)} \tag{14}$$

where X_S and X_t respectively represent the probability distributions of the source and target domains, x_s^i and x_j^t are samples from their respective domains, n_s and n_t are sample quantities, and $\phi(\cdot)$ is the mapping function. The closer S is to 1, the smaller the inter-domain difference; the closer it is to 0, the greater the difference.

3. Experimental data preprocessing

3.1 IEEE PHM 2014 Data Challenge

The aging experiment was conducted on two fuel cell stacks, each comprising 5 single cells with an active area of 100 cm^2 per cell [37]. Fuel Cell 1 (FC1) operated under a static load (current density = 0.7 A/cm^2) for 1154 hours, while Fuel Cell 2 (FC2) underwent pseudo-dynamic loading at the same current density (frequency = 5 kHz, current ripple = 10%) for 1020 hours [38]. Their maximal current density is 1 A/cm^2.

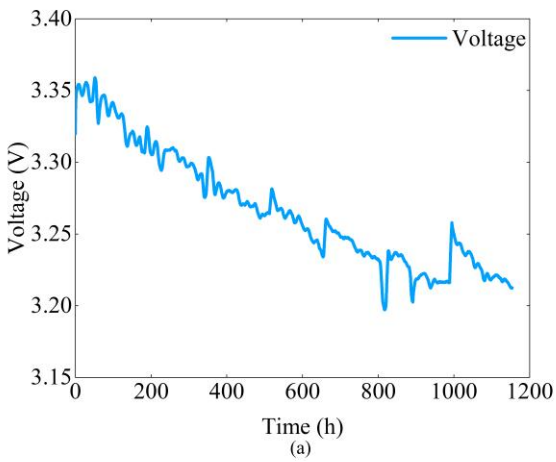

Fig. 5. Filtered voltages of (a) FC1 and (b) FC2.

Table 1 presents the ranges of physical parameters involved in the experimental setup for FC1 and FC2. Raw voltage data is preprocessed with a sampling rate of 3 data points per hour, followed by smoothing via the moving average method. The resulting voltage degradation trajectories of FC1 and FC2 are shown in Fig. 5.

Table 1 Range of physical parameters controlled (FC1 and FC2).

Parameter	Value range
Cooling flow	0 ~ 10 L/min
Cooling temperature	20 ~ 80℃
Gas humidification	0 ~ 100 % RH
Gas temperature	20 ~ 80℃
Air flow	0 ~ 100 L/min
H_2 flow	0 ~ 30 L/min
Gas pressure	0 ~ 2 bar
Fuel cell current	0 ~ 300 A

3.2 Dynamic operational data from G20 test station

The dynamic operational data was obtained from experiments conducted on the G20 test station, with the fuel cell stack designated as FC3 [39]. The single fuel cell has a seven-layer (five-layer and two-sub-gasket layers) structure, which is mainly designed for automotive applications. The basic technical parameters of the FC3 are listed in

Table 2. Specific operational parameters are presented in Table 3.

Table 2 Basic technical parameters of ingle cell (FC3).

Parameter	Value
Rated current (A)	35.6
Cell activate area (cm^2)	5*5
Thickness of membrane (mm)	0.015
Radius of Pt particle (nm)	3.2
Thickness of CL (mm)	0.006-0.008
Pt loading of the anode ($mg*cm^{-2}$)	JM Pt/C 0.1
Pt loading of the cathode ($mg*cm^{-2}$)	JM Pt/C 0.4
Pt/C catalyst loading (%)	Pt (20–50)

The experiment comprised 3076 dynamic load cycles (FC-DLC) over 1008 hours. Each cycle consists of nine tests at different load currents, corresponding to 0%, 5%, 12.5%, 26.7%, 29.2%, 41.7%, 58.3%, 83.3%, and 100% of the rated operating current. Every 304 FC-DLC cycles, the system underwent a 12-hour shutdown period where FC3 rested while the G20 station was offline, followed by polarization testing before resuming durability testing.

Table 3 Optimal parameters for PEMFC operation (FC3).

Parameter	Value
Temperature (℃)	85
Anode RH (%)	50
Cathode RH (%)	80
Air stoichiometry	3.5
Reactant inletpressure (KPa)	110

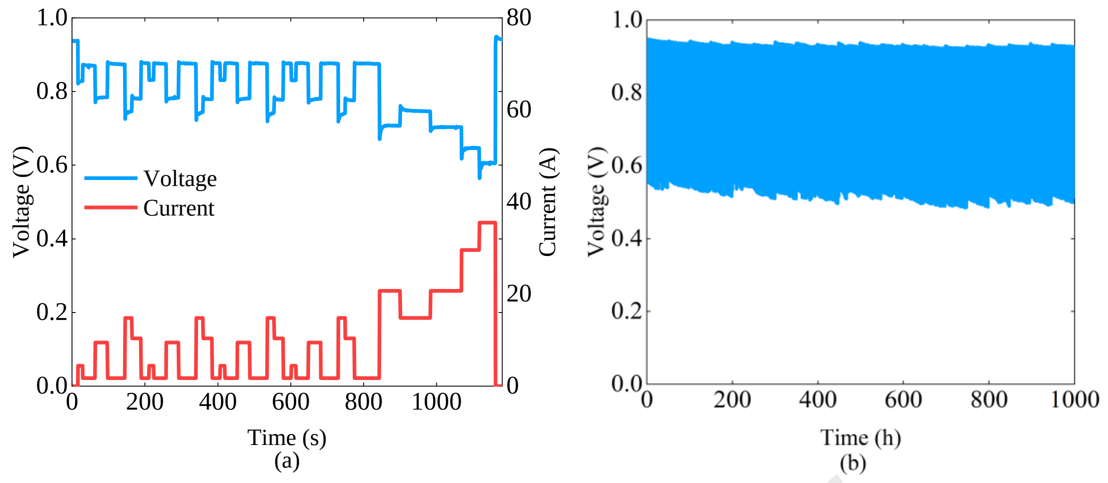

Fig. 6. Measured current and voltage profiles. (a) Current and voltage profiles of a single cycle. (b) Voltage profile of all cycles

3.3 Evaluation criteria of prediction performance

To determine the predicting performance, this paper evaluates and compares the forecasting performance of each method based on multiple indicators: Root Mean Square Error (RMSE), Mean Absolute Percentage Error (MAPE) and Coefficient of Determination (R^2).

$$RMSE = \sqrt{\frac{1}{N}\sum_{i=1}^{N}\left(y_i - y_i\right)^2} \tag{15}$$

$$MAPE = \frac{100}{N}\sum_{i=1}^{N}\left|\frac{y_i - y_i}{y_i}\right| \tag{16}$$

$$R^2 = 1 - \frac{\sum_{i=1}^{N}\left(y_i - \hat{y}_i\right)^2}{\sum_{i=1}^{N}\left(y_i - \bar{y}_i\right)^2} \tag{17}$$

where N is the number of test data, y_i is the real value, and $\hat{y}_i$ is the predicted value.

4. Results and discussion

This section first validates the superiority of the time-frequency fusion algorithm in predicting PEMFC performance degradation across multiple dimensions. For cross-domain voltage data, the LCK-TL technique proposed in Section 2.3.2 is adopted to address data distribution discrepancies between the source and target domains. Finally, the transfer prediction performance under cross-operational conditions and cross-device scenarios is discussed, achieving online prediction in dynamic operating environments. The processor of device is the 12th Gen Intel(R) Core(TM) i5-12500H. The Python version used is 3.11.

4.1 Validation of time-frequency fusion mechanism

During PEMFC operation under sufficient fuel supply, long-term aging of internal components manifests as voltage decay and output performance degradation. Different voltage frequency bands exhibit distinct impacts on fuel cell components and aging consequences. The low-frequency band (0.01 Hz–1 Hz), containing over 70% of aging-sensitive features, is critical for characterizing degradation trends. These features encompass dominant aging processes such as water transport in gas diffusion layers and membrane hydration [40]. This section analyzes the effectiveness of the time-frequency fusion mechanism in TimesNet-LSTM.

4.1.1 Interpretability of time-frequency fusion

The TimesBlock module adaptively extracts dominant low-frequency features from PEMFC voltage signals by adjusting the *top_k* parameter. Fig. 7 illustrates the frequency feature extraction and reconstruction processes for three operational datasets. Compared to the steady-state operation of FC1 and FC2, dynamically loaded FC3 exhibits steeper spectral peaks due to transient conditions, yet all three datasets demonstrate primary energy concentration in the low-frequency band. Low-frequency voltage features fluctuations inherently correlate with core PEMFC mechanisms, where amplitude-frequency characteristics are governed by membrane hydration dynamics and proton conduction efficiency, quantitatively reflecting the intrinsic timescales of electrochemical responses. Notably, residual high-frequency components in FC3 indicate incomplete smoothing of stochastic noise or transient fluctuations during preprocessing. The *top_k* optimization mechanism in TimesNet-LSTM suppresses such interference, enabling robust assessment of PEMFC performance degradation.

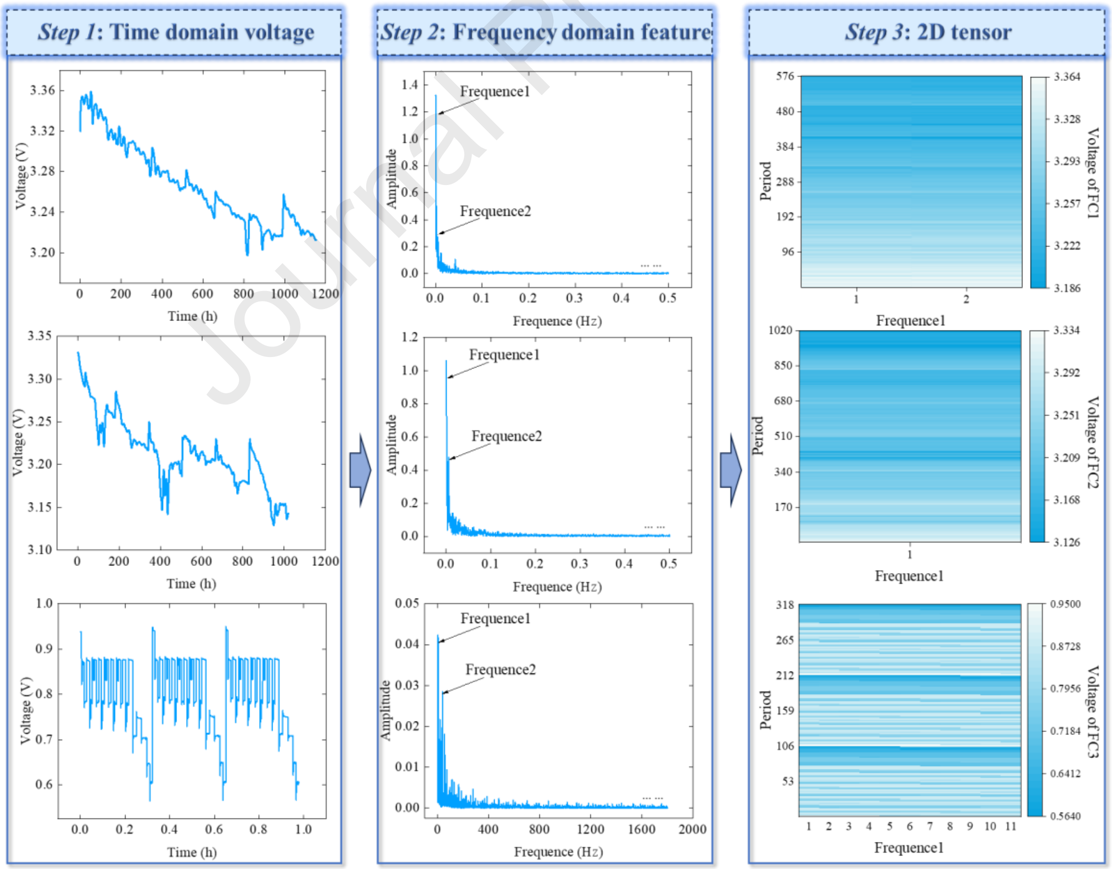

Fig. 7. Frequency-domain 2D tensor transformation.

4.1.2 Superiority validation of TimesNet-LSTM

This section selects dynamic operational data (FC3) to analyze the prediction performance of TimesNet-LSTM. Reference [23] extensively compares TimesNet with over ten advanced algorithms, including RNN-based, CNN-based, and Transformer-based models, validating its superiority across short-term and long-term prediction tasks. Therefore, this section primarily contrasts the superiority of TimesNet-LSTM with TimesNet.

Table 4 Hyperparameter setting of TimesNet module.

Model parameter	*e_layers*	*batch_size*	*d_model*	*d_ff*	*num_kernels*	*dropout*
	2	32	32	32	6	0.1

The models are trained using training ratios of 0.5, 0.6, 0.7, and 0.8. For TimesNet, the input sequence length and number of iterations are both set to 60, while other hyperparameters follow the default configuration validated by Wu et al. [23] across multiple time-series forecasting tasks (in Table 4). The remaining hyperparameters were determined through extensive ablation studies.

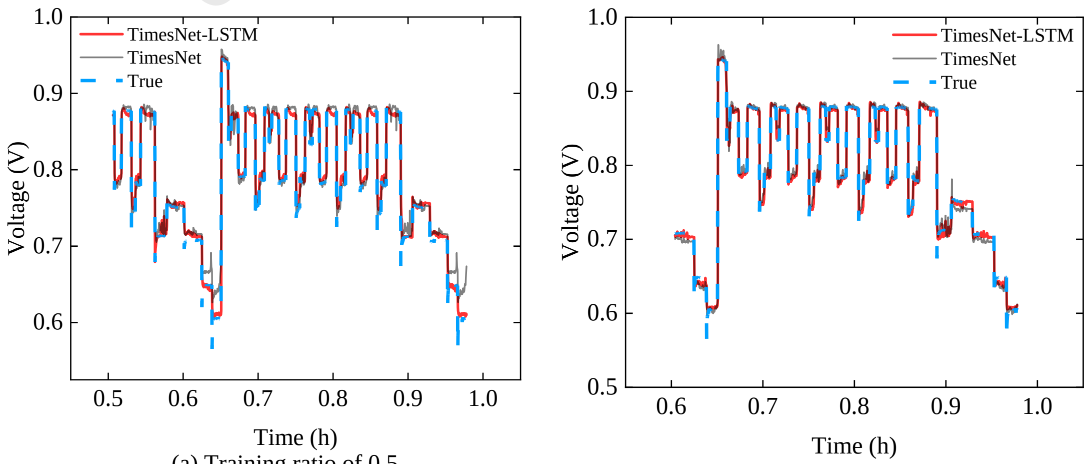

(a) Training ratio of 0.5 (b) Training ratio of 0.6

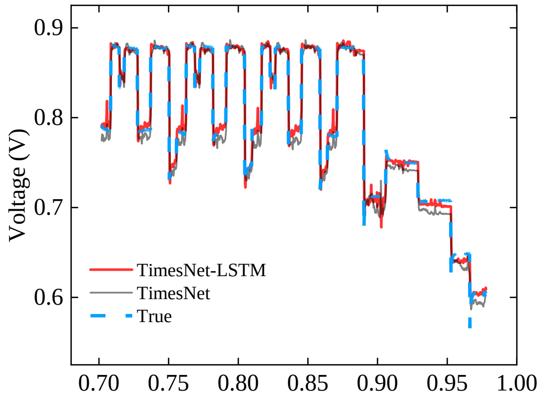

(c) Training ratio of 0.7

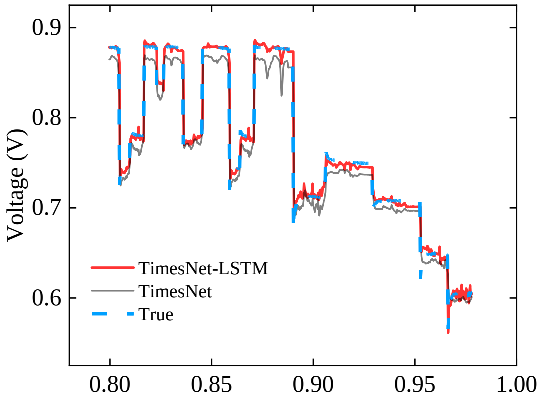

(d) Training ratio of 0.8

Fig. 8. Predictions of TimesNet-LSTM under different training ratios.

Fig. 8 presents the prediction results on the FC3 dataset. Under different training ratios, both models effectively capture key voltage extremes and follow the overall degradation trend. However, in regions with pronounced dynamic fluctuations, TimesNet exhibits noticeable phase lag when detecting abrupt voltage changes, due to its lack of a temporal gating mechanism. In contrast, TimesNet-LSTM substantially mitigates such deviations through the gated forgetting mechanism of LSTM, confirming that temporal memory enhances frequency-domain analysis. Further analysis reveals that the time-frequency collaboration in TimesNet-LSTM leads to more consistent tracking of voltage trends. As per Table 5 (training ratio = 0.8), TimesNet-LSTM reduces RMSE and MAPE by 9.7% and 39.9%, respectively, compared to TimesNet. The aforementioned results demonstrate the superior prediction performance of TimesNet-LSTM across varying training ratios. The following analysis validates the superiority of TimesNet-LSTM through different prediction steps, with a fixed training ratio of 0.5 and step sizes of 5, 10, 50, and 100, using RMSE as the evaluation metric.

Table 5 Comparison of prediction accuracy (FC3).

Training ratio	Model	RMSE	MAPE
0.5	TimesNet	0.01841	1.13575
	TimesNet-LSTM	0.01732	1.06541
0.6	TimesNet	0.01773	1.01931
	TimesNet-LSTM	0.01631	0.72943
0.7	TimesNet	0.01663	1.18904
	TimesNet-LSTM	0.01432	0.6982
0.8	TimesNet	0.01503	1.08745
	TimesNet-LSTM	0.01357	0.65371

As shown in Fig. 9, prediction accuracy declines for both models as the step size increases. However, TimesNet-LSTM consistently outperforms TimesNet at identical step sizes. Furthermore, TimesNet-LSTM achieves the smallest error area, highlighting its robust prediction stability.

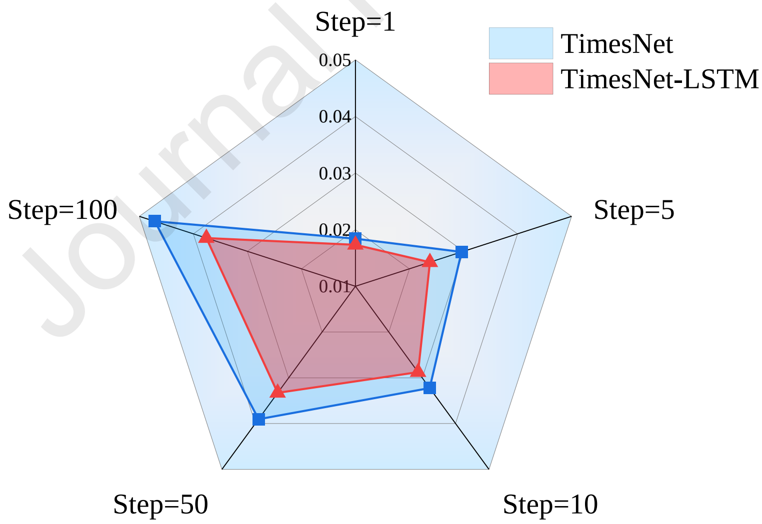

Fig. 9. Predictions of TimesNet-LSTM under different inputs.

In summary, TimesNet-LSTM delivers enhanced prediction performance through its time-frequency collaboration mechanism. Multi-dimensional analyses comprehensively validate the synergistic representation advantages of the dual-stream architecture for degradation features, underscoring the superiority of the time-frequency fusion in TimesNet-LSTM. Compared to TimesNet, TimesNet-LSTM reduces RMSE and MAPE by 5.9%−13.9% and 6.2%−41.3%, respectively.

4.2 Low-frequency consensus knowledge-based transfer learning

To validate the transfer effectiveness of the LCK-TL model, FC1 and FC2 are assigned as the source domain, while FC3 serves as the target domain. The *S* metric quantifies inter-domain similarity under varying *top_k* values, where a score approaching 1 indicates higher distribution discrepancies.

Table 6 The *S* values under different combinations.

The value of *top_k*	Source: FC1 Target: FC3	Source: FC2 Target: FC3
0 (Origin data)	0.875	0.854
1	-	-
2	0.999	0.999
3	0.889	0.842
4	0.941	0.891
5	0.927	0.985
6	0.897	0.987
7	0.892	0.986

The quantitative results are presented in Table 6. Setting *top_k* to 1 restricts feature extraction to the 0 Hz DC component, which corresponds to the signal mean. Under this condition, the extracted features cannot adequately represent the periodic characteristics of the voltage time series. Therefore, quantitative analysis is not performed. Additionally, raw data exhibits the most significant domain shifts (*top_k* = 0) due to inherent differences between steady-state and dynamic conditions. Conversely, the value of *S* peaks at *top_k* = 2, demonstrating effective alignment of dominant frequency fluctuation features between domains, thereby bridging feature distribution discrepancies across operating conditions and providing optimal frequency-domain feature selection for cross-domain transfer models. To validate the optimization effect at *top_k* = 2, 2D feature distribution visualization is performed via the KDE module in LCK-TL. Fig. 10(a) reveals significant distribution shifts between the steady-state source domain and dynamic target domain in raw data. After LCK-TL feature reconstruction, Fig. 10(b) shows highly overlapping cross-domain distributions.

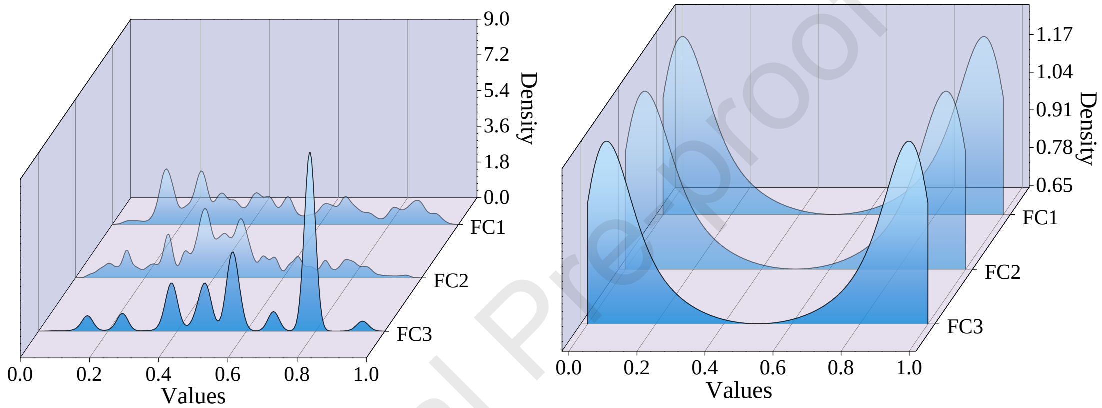

(a) Original distribution (b) The distribution after LCK-TL

Fig. 10. Distribution results of LCK-TL.

The distribution visualization and quantitative S values objectively characterize the distribution discrepancies between domains. The key contribution of the LCK-TL is its capability to actively construct a consensus feature space that mitigates the impact of these inherent cross-condition variations. The highly overlapping distributions after processing demonstrate that LCK-TL effectively identifies and aligns domains by extracting domain-invariant low-frequency features, rather than merely compensating for a severe shift. These results confirm that the proposed method enhances the robustness and stability of the prediction model against operational distribution changes, significantly improving the cross-domain generalization capability compared to traditional TL methods.

4.3 Cross-condition and cross-device transfer prediction

This section implements cross-condition and cross-device transfer prediction via transfer learning, where FC1 and FC2 serve as source domain data, and FC3 as the target domain. Under basic transfer learning, the source models trained on FC1 and FC2 are designated as TL_1 and TL_2. For LCK-TL, the corresponding models are LCK-TL_1 and LCK-TL_2. The prediction performance of LCK-TL and basic TL is first compared in offline prediction mode, followed by an investigation of online prediction under dynamic conditions.

4.3.1 Offline prediction based LCK-TL

Building on the validity of LCK-TL demonstrated in Section 4.2, this section simulates offline prediction applications via single-step forecasting to further analyze LCK-TL's performance under dynamic conditions. Using FC2 as the source domain and FC3 as the target domain, Fig. 11 compares the prediction results of direct training, TL_2, and LCK-TL_2.

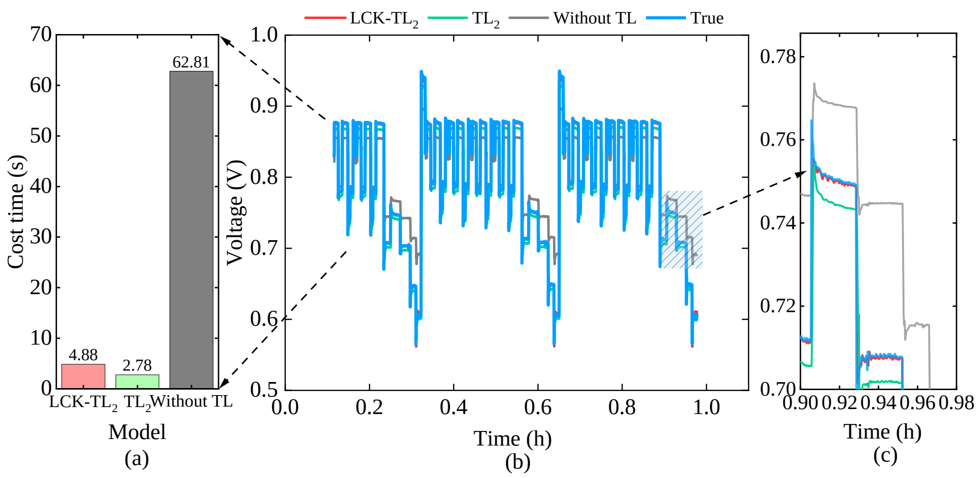

Fig. 11. Offline prediction results of TL_2 and LCK-TL_2

As shown in Fig. 11(b), the TimesNet-LSTM model without transfer learning exhibits significant prediction deviations under 10% training data, particularly during rapid load changes in late-stage dynamic operations. Additionally, the extended training time fails to meet online prediction timeliness requirements. LCK-TL_2 eliminates the need for model training on the target domain, thereby reducing the computational cost to solely the inference time during the prediction phase. Although LCK-TL_2 introduces a 2-second latency due to cross-domain feature alignment, it increases R^2 by 12.1% and reduces RMSE and MAPE by 42.1% and 54.8%, respectively, through low-frequency consensus feature extraction. Thus, LCK-TL achieves significant accuracy improvements while retaining the inherent low-latency advantages of transfer learning.

Table 7 Performance of each prediction model under dynamic conditions.

Model	RMSE	MAPE	R^2	Runtime (s)
TL_1	0.04050	3.13822	0.801	2.63
TL_2	0.03227	2.09538	0.851	2.78
LCK-TL_1	0.01909	0.93696	0.952	4.91
LCK-TL_2	0.01868	0.94722	0.954	4.88

Table 7 compares the prediction accuracy of TL_1, TL_2, LCK-TL_1, and LCK-TL_2 models. The data indicate that the LCK-TL framework consistently achieves optimal performance, which is attributed to its domain-invariant feature mining mechanism via low-frequency consensus knowledge transfer. Notably, TL_1 and TL_2 exhibit significant fluctuations in prediction deviation, with a difference in R^2 of 6.2%. This result highlights the high sensitivity of traditional transfer learning to discrepancies between source and target domain distributions. In contrast, performance variations among

LCK-TL models converge within 0.2%.

By extracting cross-domain invariant low-frequency features, LCK-TL simultaneously attenuates domain discrepancies and enhances source domain universality, enabling the construction of generalized degradation prediction architectures without requiring specific source domain selection. This provides theoretical guarantees for the rapid deployment of online prediction systems.

4.3.2 Online prediction under dynamic conditions

Online prediction requires timely assessment of future operational fluctuations. As traditional single-step prediction lacks anticipatory capability for dynamic processes, this section validates LCK-TL's online prediction results via multi-step forecasting simulations. Based on the offline prediction analysis of LCK-TL in Section 4.3.1, LCK-TL_2 is selected as the source model. Unlike Section 4.3.1, LCK-TL_2 is trained in multi-step prediction mode. Fig. 12 illustrates the online prediction results of LCK-TL_2 at a prediction step size of 50 and 80.

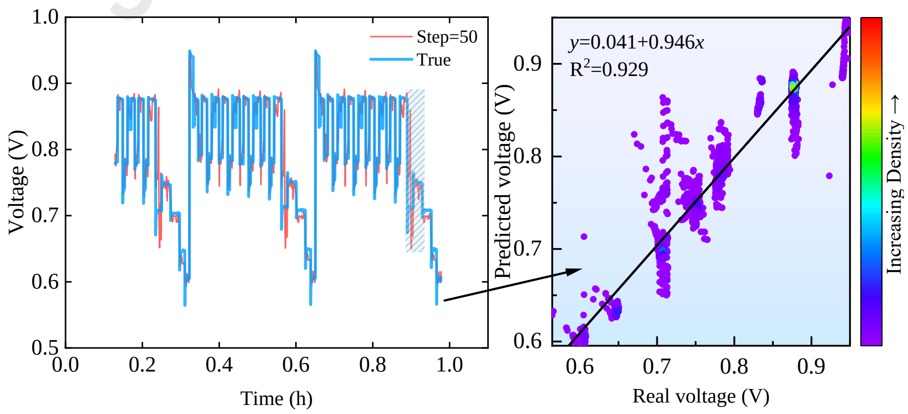

(a)

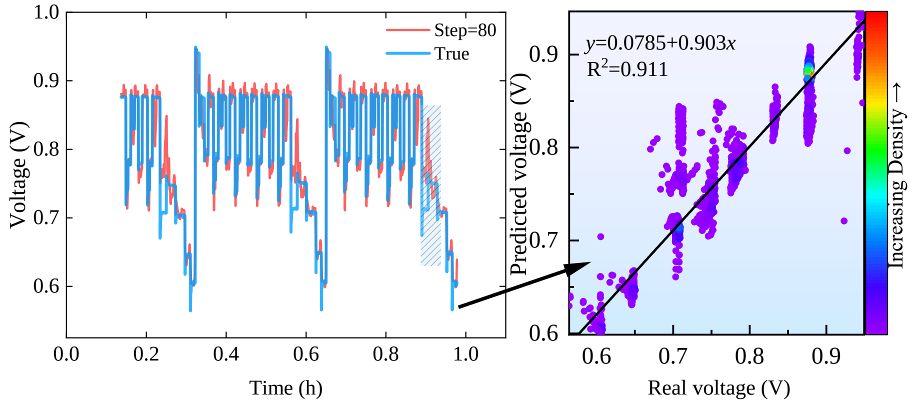

(b)

Fig. 12. Online prediction result of LCK-TL2.

As shown in Fig. 12(a), LCK-TL2 demonstrates strong temporal extrapolation capability at 50 steps, achieving $R^2 = 0.929$ (only 2.6% degradation compared to single-step prediction), indicating effective suppression of error accumulation in multi-step forecasting. At 80 prediction steps, LCK-TL2 maintains high accuracy with an R^2 of 0.911. However, it does not fully capture voltage trends during abrupt load drops, as visible in the shaded regions. Performance further declines at 100 steps, where the R^2 value drops to 0.788, as summarized in Table 8. Importantly, computational efficiency remains stable, with inference times consistently under 5 seconds, meeting typical real-time requirements. Considering FC3's sampling frequency and dataset scale, these results validate LCK-TL2's engineering applicability for online tasks.

Table 8 The prediction performance of LCK-TL2 under different step sizes.

Step	RMSE	MAPE	R^2	Cost time(s)
1	0.01868	0.94722	0.954	4.88
5	0.02189	1.44959	0.943	4.73
10	0.02048	1.55654	0.941	4.91
50	0.02255	1.73519	0.929	4.94
80	0.02553	1.88886	0.911	4.92
100	0.03919	3.09689	0.788	4.89

To further validate the predictive performance of LCK-TL over longer operating durations, this section evaluates its performance using durability test data from the first 50 hours and the first 100 hours. Each 50-hour segment contains nearly 180,000 data points. Furthermore, since Table 8 has comprehensively discussed the impact of prediction step size on performance, a step size of 10 is selected here to verify the prediction accuracy of LCK-TL under these experimental conditions.

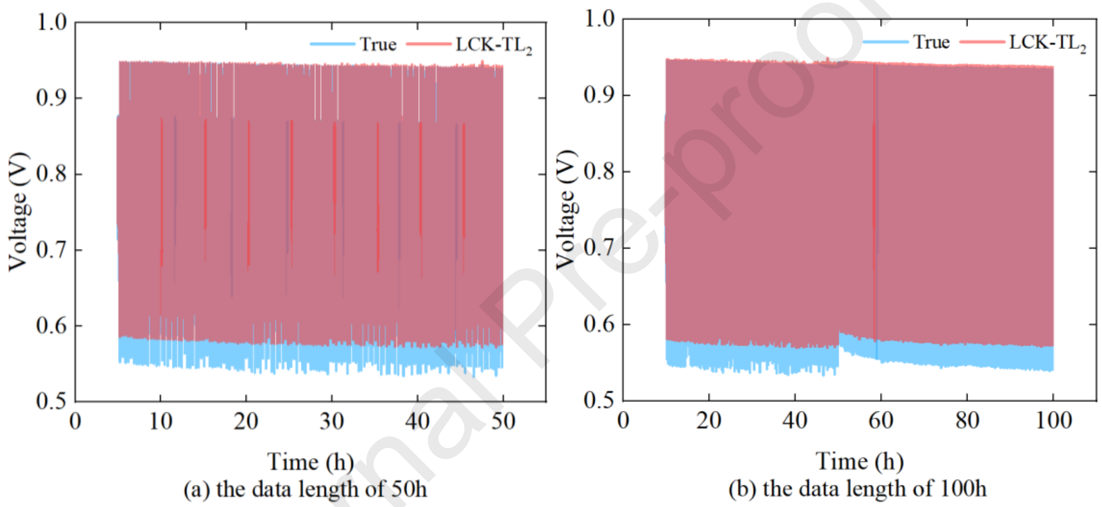

Fig. 13. Prediction results under data lengths of 50h and 100h.

As shown in Fig. 13, LCK-TL$_2$ effectively captures the voltage variation trend even during extended PEMFC operation. Regarding error metrics, for a data length of 50 hours, LCK-TL$_2$ achieves an RMSE of 0.0239 and an MAPE of 1.3731. For a data length of 100 hours, the RMSE and MAPE of LCK-TL$_2$ are 0.0241 and 1.3691, respectively. These values are comparable to the prediction errors obtained with a 1-hour data length. In terms of R^2, the values are 0.928 and 0.927 for data lengths of 50 and 100 hours, respectively, demonstrating a good model fit. The above analysis indicates that LCK-TL maintains robust transfer prediction performance across different data lengths.

4.4 Advanced analysis with cutting-edge methods

To thoroughly validate the effectiveness of LCK-TL in predicting PEMFC degradation, this study conducts a comprehensive comparison with several state-of-the-art transfer learning methods. Given the relative scarcity of transfer learning studies under dynamic fuel cell conditions, the experiments adopt a transfer task with FC1 as the source domain and FC2 as the target domain, aligning with evaluation settings commonly used in existing literature.

In addition to comparing the prediction accuracy of voltage degradation trajectories, this section introduces the relative error (RE) of RUL as an evaluation metric to more comprehensively assess the engineering practicality of each method. To ensure a fair comparison, all compared methods employ the best performance results reported in their respective original studies and are evaluated uniformly under the same transfer task. It is worth noting that differences exist in the test data length and end-of-life (EoL) threshold settings used in RUL evaluation across different methods. This study uses the ground-truth RUL values as a benchmark to ensure the fairest possible comparison.

Table 9 Comparative prediction results based on different prediction methods.

Method	RMSE	TRUE RUL (h)	Pred RUL (h)	RUL_RE (%)
LCK-TL	0.00196	225	221	1.78
	0.00212	325	329	1.23
	0.00233	425	419	1.41
TLTNN [30]	0.00598	-	-	-
FT-LSTM [28]	0.00640	-	-	-
Bi-LSTM-AM [41]	0.00303	236	232	5.04
MT-CNN-BiLSTM [42]	0.00245	225	208	7.11

FT-CNN-BiLSTM [42]	0.00239	225	209	7.56
HTL-CNN-BiLSTM [42]	0.00218	225	226	0.44
LQLSTM [43]	0.00260	224	221	1.33

Table 9 presents the prediction accuracy and RUL estimation errors of all methods. In the evaluation with a true RUL of 225 h, the proposed LCK-TL method consistently achieves the lowest RMSE in voltage prediction, while its RUL estimation error remains second only to the LQLSTM method. To rule out randomness and examine generalizability, further validation is performed under scenarios with true RUL values of 325 h and 425 h. The results demonstrate that although the accuracy of LCK-TL slightly decreases as the prediction horizon increases, its overall performance remains significantly superior to the best results obtained by existing methods over shorter prediction ranges. Moreover, the RUL estimation error consistently stays within 2%. In conclusion, these comparative results fully demonstrate the superiority and stability of the LCK-TL method in PEMFC aging prediction and lifespan assessment.

5. Conclusion

This study addresses the challenge of small-sample transfer in PEMFC degradation prediction under dynamic conditions by proposing an innovative architecture that integrates time-frequency fusion with collaborative transfer learning. The approach achieves theoretical breakthroughs in dynamic characterization, cross-domain generalization, and online prediction efficiency. At the algorithmic level, the TimesNet-LSTM network is developed to overcome the limitations of single-domain prediction methods. By integrating its low-frequency feature extraction capability with transfer learning, the LCK-TL technique is introduced to enable generalized prediction across varying operating conditions and devices. Leveraging the rapid-response and low computational advantages of transfer learning, the proposed method enables efficient multi-step online prediction. Key findings are summarized as follows:

1) The TimesNet-LSTM architecture combines TimesNet's multi-period frequency-domain representation with LSTM's temporal dynamic memory mechanism. Compared to TimesNet, TimesNet-LSTM reduces RMSE and MAPE by 5.9%−13.9% and 6.2%−41.3%, respectively.

2) LCK-TL effectively reduces inter-domain data distribution discrepancies by extracting low-frequency consensus knowledge from PEMFCs. Compared to traditional transfer learning techniques, LCK-TL improves R^2 by 12.1% and reduces RMSE and MAPE by 42.1% and 54.8%, respectively.

3) Compared to the strong sensitivity of traditional transfer learning to source-target domain distribution differences (R^2 difference reaches 6.2%), the performance variations among LCK-TL models converge within 0.2%. LCK-TL effectively achieves domain discrepancy attenuation and enhanced source domain universality without requiring specific source domain screening, enabling the construction of generalized prediction architectures.

4) LCK-TL maintains robust prediction performance within 100 steps, with computational costs consistently below 5 s. These results validate the feasibility of LCK-TL for rapid deployment in online prediction systems.

Although this study achieves fast and accurate prediction under cross-device and cross-operating-condition scenarios, there remains a gap between the experimental conditions of the testing platform and real-world vehicular environments. Additionally, performance degradation is observed in multi-step predictions with extra-long horizons. In the future, we will focus on developing an adaptive feature selection algorithm to achieve self-calibration for inter-domain discrepancies. This will further enhance the feasibility of deploying cross-domain online prediction in real vehicular environments.

References

[1] Zhu W, Li Y, Xu Y, Zhang L, Guo B, Xiong R, et al. Interval prediction of fuel cell degradation based on voltage signal frequency characteristics with TimesNet-GPR under dynamic conditions. Journal of Cleaner Production 2025;486:144503. https://doi.org/10.1016/j.jclepro.2024.144503.

[2] Jia C, Liu W, Chau KT, He H, Zhou J, Niu S. Passenger-aware reinforcement learning for efficient and robust energy management of fuel cell buses. eTransportation 2026;27:100537. https://doi.org/10.1016/j.etran.2025.100537.

[3] Meng X, Sun C, Mei J, Tang X, Hasanien HM, Jiang J, et al. Fuel cell life prediction considering the recovery phenomenon of reversible voltage loss. Journal of Power Sources 2025;625:235634. https://doi.org/10.1016/j.jpowsour.2024.235634.

[4] Zuo J, Steiner NY, Li Z, Hissel D. Health management review for fuel cells: Focus on action phase. Renewable and Sustainable Energy Reviews 2024;201:114613. https://doi.org/10.1016/j.rser.2024.114613.

[5] Zhou J, Shu X, Zhang J, Yi F, Jia C, Zhang C, et al. A deep learning method based on CNN-BiGRU and attention mechanism for proton exchange membrane fuel cell performance degradation prediction. International Journal of Hydrogen Energy 2024;94:394–405. https://doi.org/10.1016/j.ijhydene.2024.11.127.

[6] Jia C, He H, Zhou J, Li K, Li J, Wei Z. A performance degradation prediction model for PEMFC based on bi-directional long short-term memory and multi-head self-attention mechanism. International Journal of Hydrogen Energy 2024;60:133–46. https://doi.org/10.1016/j.ijhydene.2024.02.181.

[7] Zhang T, Hou Z, Li X, Chen Q, Wang Q, Lüddeke C, et al. A novel multivariable prognostic approach for PEMFC degradation and remaining useful life prediction using random forest and temporal convolutional network. Applied Energy 2025;385:125569. https://doi.org/10.1016/j.apenergy.2025.125569.

[8] Liu Y, Qie T, Feng W, Iu HHC, Fernando T, Wei Z, et al. A Novel Barrier Lyapunov Function-Based Online Learning Control Method for Solid Oxide Fuel Cell in DC Microgrids. IEEE Transactions on Smart Grid 2025;16:2774–90. https://doi.org/10.1109/TSG.2025.3567616.

[9] Liu Y, Wang R, Feng W, Li R, Wei Z, Iu HHC, et al. A Stable Recurrent Equilibrium Network-Based Controller for Proton Exchange Membrane Fuel Cell in DC Microgrids. IEEE Transactions on Smart Grid 2025;16:4348–65. https://doi.org/10.1109/TSG.2025.3589801.

[10] Zhu W. High accuracy and adaptability of PEMFC degradation interval prediction

with Informer-GPR under dynamic conditions 2024.

[11] Chen K, Laghrouche S, Djerdir A. Remaining Useful Life Prediction for Fuel Cell Based on Support Vector Regression and Grey Wolf Optimizer Algorithm. IEEE Trans Energy Convers 2022;37:778–87. https://doi.org/10.1109/TEC.2021.3121650.

[12] He K, Liu Z, Sun Y, Mao L, Lu S. Degradation prediction of proton exchange membrane fuel cell using auto-encoder based health indicator and long short-term memory network. International Journal of Hydrogen Energy 2022;47:35055–67. https://doi.org/10.1016/j.ijhydene.2022.08.092.

[13] Wu H, Wang W, Li Y, Zhu W, Xie C, Gooi HB. Hybrid Physics-Based and Data-Driven Prognostic for PEM Fuel Cells Considering Voltage Recovery. IEEE Trans Energy Convers 2023:1–11. https://doi.org/10.1109/TEC.2023.3311460.

[14] Wu H, Fan F, Song K, Sun C, Li Y, Xie C, et al. Reliable cross-domain lifetime prediction for fuel cells: A time-frequency fusion transfer learning architecture. Energy 2026;344:139854. https://doi.org/10.1016/j.energy.2025.139854.

[15] Sun B, Liu X, Wang J, Wei X, Yuan H, Dai H. Short-term performance degradation prediction of a commercial vehicle fuel cell system based on CNN and LSTM hybrid neural network. International Journal of Hydrogen Energy 2023;48:8613–28. https://doi.org/10.1016/j.ijhydene.2022.12.005.

[16] Wang C, Li Z, Outbib R, Dou M, Zhao D. Symbolic deep learning based prognostics for dynamic operating proton exchange membrane fuel cells. Applied

Energy 2022;305:117918. https://doi.org/10.1016/j.apenergy.2021.117918.

[17] Liu H, Chen J, Hissel D, Hou M, Shao Z. A multi-scale hybrid degradation index for proton exchange membrane fuel cells. Journal of Power Sources 2019;437:226916. https://doi.org/10.1016/j.jpowsour.2019.226916.

[18] Li S, Luan W, Wang C, Chen Y, Zhuang Z. Degradation prediction of proton exchange membrane fuel cell based on Bi-LSTM-GRU and ESN fusion prognostic framework. International Journal of Hydrogen Energy 2022;47:33466–78. https://doi.org/10.1016/j.ijhydene.2022.07.230.

[19] Peng W, Wei Z, Huang C-G, Feng G, Li J. A Hybrid Health Prognostics Method For Proton Exchange Membrane Fuel Cells With Internal Health Recovery. IEEE Trans Transp Electrific 2023:1–1. https://doi.org/10.1109/TTE.2023.3243788.

[20] Wu H, Xu J, Wang J, Long M. Autoformer: Decomposition Transformers with Auto-Correlation for Long-Term Series Forecasting 2022. https://doi.org/10.48550/arXiv.2106.13008.

[21] Wang C, Dou M, Li Z, Outbib R, Zhao D, Zuo J, et al. Data-driven prognostics based on time-frequency analysis and symbolic recurrent neural network for fuel cells under dynamic load. Reliability Engineering & System Safety 2023;233:109123. https://doi.org/10.1016/j.ress.2023.109123.

[22] Wu H, Zhang R, Zhu W, Xie C, Li Y, Yang Y, et al. A health index-based approach for fuel cell lifetime estimation. iScience 2024;27:110979. https://doi.org/10.1016/j.isci.2024.110979.

[23] Wu H, Hu T, Liu Y, Zhou H, Wang J, Long M. TIMESNET: TEMPORAL 2D-VARIATION MODELING FOR GENERAL TIME SERIES ANALYSIS 2023.

[24] Sun B, Liu X, Wang J, Wei X, Yuan H, Dai H. Short-term performance degradation prediction of a commercial vehicle fuel cell system based on CNN and LSTM hybrid neural network. International Journal of Hydrogen Energy 2023;48:8613–28. https://doi.org/10.1016/j.ijhydene.2022.12.005.

[25] Meng X, Liu M, Mei J, Li X, Grigoriev S, Hasanien HM, et al. Polarization loss decomposition-based online health state estimation for proton exchange membrane fuel cells. International Journal of Hydrogen Energy 2025;157:150162. https://doi.org/10.1016/j.ijhydene.2025.150162.

[26] Zhuang F, Qi Z, Duan K, Xi D, Zhu Y, Zhu H, et al. A Comprehensive Survey on Transfer Learning. Proceedings of the IEEE 2021;109:43–76. https://doi.org/10.1109/JPROC.2020.3004555.

[27] Zhang X, Yue J, Huang L, Qiu D, Jiang Y. An enhanced transfer learning based on addernet and deep domain confusion for prognostic of proton exchange membrane fuel cells. International Journal of Hydrogen Energy 2024;77:795–807. https://doi.org/10.1016/j.ijhydene.2024.06.090.

[28] Zhang Y, Ma R, Xie R, Feng Z, Liang B, Li Y. A Degradation Prediction Method for PEM Fuel Cell Based on Deep Temporal Feature Extraction and Transfer Learning. IEEE Transactions on Transportation Electrification 2023:1–1. https://doi.org/10.1109/TTE.2023.3262588.

[29] Yue M, Benaggoune K, Meng J, Diallo D. Implementation of an Early Stage Fuel Cell Degradation Prediction Digital Twin Based on Transfer Learning. IEEE Trans Transp Electrific 2023;9:3308–18. https://doi.org/10.1109/TTE.2022.3229716.

[30] Tang X, Qin X, Wei K, Xu S. A novel online degradation model for proton exchange membrane fuel cell based on online transfer learning. International Journal of Hydrogen Energy 2023;48:13617–32. https://doi.org/10.1016/j.ijhydene.2022.12.260.

[31] Izadi MJ, Hassani P, Raeesi M, Ahmadi P. A novel WaveNet-GRU deep learning model for PEM fuel cells degradation prediction based on transfer learning. Energy 2024;293:130602. https://doi.org/10.1016/j.energy.2024.130602.

[32] Zuo J. Long-term dynamic durability test datasets for single proton exchange membrane fuel cell. Data in Brief 2021.

[33] Zhu D, Yang Y, Pei F, Ma T. High-precision identification of polarization processes of distribution of relaxation times by polarization curve model for proton exchange membrane fuel cell. Energy Conversion and Management 2022;268:115994. https://doi.org/10.1016/j.enconman.2022.115994.

[34] Ma R, Xie R, Xu L, Huangfu Y, Li Y. A Hybrid Prognostic Method for PEMFC With Aging Parameter Prediction. IEEE Trans Transp Electrific 2021;7:2318–31. https://doi.org/10.1109/TTE.2021.3075531.

[35] Guo D, Yang G, Han X, Feng X, Lu L, Ouyang M. Parameter identification of fractional-order model with transfer learning for aging lithium-ion batteries.

International Journal of Energy Research 2021;45:12825–37. https://doi.org/10.1002/er.6614.

[36] Hu R, Wang X, Ding X, Zhang Y, Xin X, Pang W, et al. Unsupervised Domain Adaptation for Skeleton Recognition With Fourier Analysis. IEEE Internet of Things Journal 2024;11:40166–75. https://doi.org/10.1109/JIOT.2024.3450929.

[37] Pan R, Yang D, Wang Y, Chen Z. Performance degradation prediction of proton exchange membrane fuel cell using a hybrid prognostic approach. International Journal of Hydrogen Energy 2020;45:30994–1008. https://doi.org/10.1016/j.ijhydene.2020.08.082.

[38] Li C, Lin W, Wu H, Li Y, Zhu W, Xie C, et al. Performance degradation decomposition-ensemble prediction of PEMFC using CEEMDAN and dual data-driven model. Renew Energy 2023;215:118913. https://doi.org/10.1016/j.renene.2023.118913.

[39] Zuo J, Lv H, Zhou D, Xue Q, Jin L, Zhou W, et al. Deep learning based prognostic framework towards proton exchange membrane fuel cell for automotive application. Applied Energy 2021;281:115937. https://doi.org/10.1016/j.apenergy.2020.115937.

[40] Benouioua D, Candusso D, Harel F, François X, Picard P. Characterization of low and high frequency phenomena in a PEM fuel cell using singularity analysis of stack voltage. Journal of Energy Storage 2020;28:101298. https://doi.org/10.1016/j.est.2020.101298.

[41] Kebede GA, Lo S-C, Wang F-K, Chou J-H. Transfer learning-based deep learning models for proton exchange membrane fuel remaining useful life prediction. Fuel 2024;367:131461. https://doi.org/10.1016/j.fuel.2024.131461.

[42] Li Z, Yuan X, Zhang C, Mao J, Wang Y. Long-term degradation prediction method for proton exchange membrane fuel cells based on hybrid transfer learning. International Journal of Hydrogen Energy 2025;106:781–9. https://doi.org/10.1016/j.ijhydene.2025.01.405.

[43] Wang F-K, Kebede GA, Lo S-C, Woldegiorgis BH. An embedding layer-based quantum long short-term memory model with transfer learning for proton exchange membrane fuel stack remaining useful life prediction. Energy 2024;308:133054. https://doi.org/10.1016/j.energy.2024.133054.

- 2D frequency analysis integrated with 1D temporal memory for PEMFC prognostics.
- Co-optimization framework integrating prognostics and transfer learning.
- Domain discrepancy reduction via low-frequency voltage characteristics.
- Online cross-domain knowledge transfer for accurate PEMFC degradation prediction.

Declaration of interests

☒ The authors declare that they have no known competing financial interests or personal relationships that could have appeared to influence the work reported in this paper.

☐The authors declare the following financial interests/personal relationships which may be considered as potential competing interests: